

Toward a measurement of the effective gauge field and the Born-Huang potential with atoms in chip traps

Zeynep Nilhan Gürkan,¹ Erik Sjöqvist,² Björn Hessmo,^{3,4} and Benoît Grémaud^{5,4}

¹*College of Engineering and Technology, American University of the Middle East, Egaila, 54200, Kuwait*

²*Department of Physics and Astronomy, Uppsala University, Box 516, Se-751 20 Uppsala, Sweden*

³*Department of Applied Physics, Royal Institute of Technology, Se-106 91, Stockholm, Sweden*

⁴*Centre for Quantum Technologies, National University of Singapore, 2 Science Drive 3, 117542 Singapore*

⁵*Aix Marseille Univ, Université de Toulon, CNRS, CPT, IPhU, AMUTech, Marseille, France*

We study magnetic traps with very high trap frequencies where the spin is coupled to the motion of the atom. This allows us to investigate how the Born-Oppenheimer approximation fails and how effective magnetic and electric fields appear as the consequence of the non-adiabatic dynamics. The results are based on exact numerical diagonalization of the full Hamiltonian describing the coupling between the internal and external degrees of freedom. The position in energy and the decay rate of the trapping states correspond to the imaginary part of the resonances of this Hamiltonian are computed using the complex rotation method.

I. INTRODUCTION

Magnetic trapping is one of the workhorses for cold atom physics. A commonly used trap is the Ioffe-Pritchard trap [1], in which the magnetic field is non-zero at the center to prevent Majorana transitions to scattering states. In most situations, it is highly desirable to obtain high trapping frequencies and gradients for fast thermalization and strong confinement of the atoms. One method to reach high frequencies is to miniaturize the magnetic trap by using microfabricated chips [2]; a widely used setup for studying adiabatic dynamics in atomic systems [3]. This far most magnetic traps operate in a regime where the atomic spin can adiabatically follow local changes in the magnetic field. Before atoms are lost, the dynamics will be influenced by corrections to the adiabatic approximation. One such example would be where an atom orbits a current carrying wire. To describe losses and nonadiabatic effects in magnetic traps, it is convenient to work with waveguides to reduce the problem to two dimensions[4–7].

In this article, we analyze the situation in magnetic traps with very high trap frequencies, where the spin is coupled to the motion of the atom. This allows us to investigate how the Born-Oppenheimer approximation fails and how effective magnetic and electric fields appear as a consequence of the non-adiabatic dynamics [8–11]. The results are based on exact numerical diagonalization of the full Hamiltonian describing the coupling between the internal and external degrees of freedom. Using the complex rotation method, the position in energy and the decay rate of the trapping states corresponding to the imaginary part of the resonances of this Hamiltonian are computed [12].

II. MAGNETIC TRAPPING

A. Atoms in a magnetic field

The Hamiltonian of an atom with mass M and spin operator $\mathbf{S} = (S_x, S_y, S_z)$ in a magnetic field \mathbf{B} , is given by

$$H = \frac{\mathbf{p}^2}{2M} + \frac{g\mu_B}{\hbar} \mathbf{S} \cdot \mathbf{B}, \quad (1)$$

where μ_B is the Bohr magneton and g is the g -factor. We consider the $S = 1$ case. By writing

$$\mathbf{B} = B(\sin \alpha \cos \beta, \sin \alpha \sin \beta, \cos \alpha), \quad (2)$$

where B , α and β values are varying in space, the Hamiltonian reads

$$H = \frac{\mathbf{p}^2}{2M} + \frac{\mu_B B_{tot}}{\sqrt{2}} \begin{pmatrix} \sqrt{2} \cos \alpha & e^{-i\beta} \sin \alpha & 0 \\ e^{i\beta} \sin \alpha & 0 & e^{-i\beta} \sin \alpha \\ 0 & e^{i\beta} \sin \alpha & -\sqrt{2} \cos \alpha \end{pmatrix}, \quad (3)$$

in the eigenbasis $|-1\rangle, |0\rangle, |1\rangle$ of S_z .

When the Larmor frequency $\omega_L = \mu_B B_{tot}/\hbar$ is much larger than the typical frequency of the atomic motion, the fast spin dynamics decouple from the slow evolution of the center of mass of the atom. In the Born-Oppenheimer approximation, the state of the system $\Psi(\mathbf{r})$ is written as

$$|\Psi(\mathbf{r})\rangle \approx \psi_j(\mathbf{r})|\chi_j(\mathbf{r})\rangle, \quad (4)$$

where $\psi_j(\mathbf{r})$ is the wave function and $|\chi_j(\mathbf{r})\rangle$ is an eigenvector of the position dependent spin-part of the Hamiltonian H in Eq. (4). The effective potential seen by the atoms is just the associated eigenvalue $V_j(\mathbf{r})$, whose minimum, if existing, creates a trapping potential. In addition, since the local eigenstates $|\chi_j(\mathbf{r})\rangle$ are position

dependent a vector potential and an additional scalar potential appear, for each component $\psi_j(\mathbf{r})$:

$$\begin{aligned}\mathbf{A}_j(\mathbf{r}) &= -i\hbar\langle\chi_j(\mathbf{r})|\nabla\chi_j(\mathbf{r})\rangle, \\ \Phi_j(\mathbf{r}) &= \frac{\hbar^2}{2}[\langle\nabla\chi_j(\mathbf{r})|(1-|\chi_j(\mathbf{r})\rangle\langle\chi_j(\mathbf{r})|)\cdot|\nabla\chi_j(\mathbf{r})\rangle].\end{aligned}\quad (5)$$

These quantities are well-known in molecular physics as Berry-Mead and Born-Huang potentials [9]. In cold atomic gases, they appear in the situation of position dependent dark-states [13], allowing experimental realizations of artificial gauge fields [14]. The eigenstates $|\chi_j(\mathbf{r})\rangle$ of the spin Hamiltonian are only defined up to a phase factor, which can be position dependent. From the preceding expression, one readily obtains that the change $|\chi_j(\mathbf{r})\rangle \rightarrow e^{if(\mathbf{r})/\hbar}|\chi_j(\mathbf{r})\rangle$ amounts to the gauge transformation:

$$\begin{aligned}\mathbf{A}_j(\mathbf{r}) &\rightarrow \mathbf{A}_j(\mathbf{r}) + \nabla f(\mathbf{r}), \\ \Phi_j(\mathbf{r}) &\rightarrow \Phi_j(\mathbf{r}).\end{aligned}\quad (6)$$

In addition to these adiabatic terms, there are also couplings between the different eigenstates $|\chi_j(\mathbf{r})\rangle$, which appears as off-diagonal terms of the Hamiltonian in the $|\chi_j(\mathbf{r})\rangle$ basis. They are precisely responsible for the Majorana losses [15, 16].

B. Experimental set-up

To observe the effects of the effective Berry-Mead and Born-Huang potentials, it is required to use magnetic traps with high trap frequencies. One efficient way to realize this is to use microfabricated magnetic traps, which are formed when the magnetic field from a small current-carrying wire is superimposed with an external bias field. The magnetic field from a thin and long wire along the z -axis is given by $\mathbf{B}_\theta(r) = \frac{\mu_0}{2\pi} \frac{I_\omega}{r} \mathbf{e}_\theta$, where θ is the polar angle in cylindrical coordinates, r is the distance from the wire, and I_ω is current. We assume a homogeneous external bias field $\mathbf{B}_{\text{bias}} = (\frac{B_0}{\sqrt{2}}, -\frac{B_0}{\sqrt{2}}, B_z)$. Superimposing $\mathbf{B}_\theta(r)$ and \mathbf{B}_{bias} , we obtain, in cartesian coordinates, the total magnetic field

$$\begin{aligned}\mathbf{B} &= \left(\frac{B_0}{\sqrt{2}} - \frac{\mu_0}{2\pi} \frac{I_\omega y}{x^2 + y^2}, -\frac{B_0}{\sqrt{2}} + \frac{\mu_0}{2\pi} \frac{I_\omega x}{x^2 + y^2}, B_z\right) \\ &= (\tilde{B}_x, \tilde{B}_y, \tilde{B}_z).\end{aligned}\quad (7)$$

The magnitude of \mathbf{B} is given by

$$B^2 = B_z^2 + B_0^2 - \frac{\sqrt{2}B_0\xi(x+y)}{x^2 + y^2} + \frac{\xi^2}{x^2 + y^2} \quad (8)$$

with $\xi = \frac{\mu_0 I_\omega}{2\pi}$. This has a minimum at the position $x_0 = y_0 = \frac{\xi}{\sqrt{2}B_0}$, where weak-field seeking atoms can be trapped.

Introducing local coordinates (\tilde{x}, \tilde{y}) around the minimum (x_0, y_0) , the xy -components of the magnetic field

read:

$$\begin{aligned}\tilde{B}_x &= \frac{\frac{B_0}{\sqrt{2}}((x_0 + \tilde{x})^2 + (y_0 + \tilde{y})^2) - \xi(y_0 + \tilde{y})}{(x_0 + \tilde{x})^2 + (y_0 + \tilde{y})^2}, \\ \tilde{B}_y &= \frac{-\frac{B_0}{\sqrt{2}}((x_0 + \tilde{x})^2 + (y_0 + \tilde{y})^2) + \xi(x_0 + \tilde{x})}{(x_0 + \tilde{x})^2 + (y_0 + \tilde{y})^2},\end{aligned}\quad (9)$$

which to first order in \tilde{x} and \tilde{y} reduce to

$$\tilde{B}_x \approx \frac{B_0^2}{\xi} \tilde{x}, \quad \tilde{B}_y \approx -\frac{B_0^2}{\xi} \tilde{y}. \quad (10)$$

This approximation can be readily obtained from the linearization of \mathbf{B} at the minimum of the potential: $\mathbf{B} \approx (G\tilde{x}, -G\tilde{y}, B_z)$, where G is the gradient of the magnetic field in the (\tilde{x}, \tilde{y}) plane, i.e.,

$$G = \frac{B_0^2}{\xi} = \frac{2\pi}{\mu_0} \frac{B_0^2}{I_\omega}. \quad (11)$$

C. Harmonic units

As explained just above, weak-field seeking atoms can be trapped around the minimum of the magnetic field; more precisely, the effective trapping potential is proportional to:

$$\mu_B B = \mu_B B_z \sqrt{1 + \frac{G^2}{B_z^2} (\tilde{x}^2 + \tilde{y}^2)}, \quad (12)$$

where the harmonic approximation leads an effective trap frequency (and harmonic length)

$$\omega_T = \sqrt{\frac{\mu_B B_z}{M} \frac{G}{B_z}}, \quad \ell_T = \sqrt{\frac{\hbar}{M\omega_T}}. \quad (13)$$

Using ℓ_T and ω_T as harmonic units for length and energy and by introducing the Larmor-type frequency $\omega_L = \mu_B B_z / \hbar$, the Hamiltonian for a spin-1 reads

$$\begin{aligned}\frac{H}{\hbar\omega_T} &= \frac{\mathbf{p}^2}{2} \\ &+ \frac{V(\mathbf{r})}{\sqrt{2}} \begin{pmatrix} \sqrt{2} \cos \alpha & e^{-i\beta} \sin \alpha & 0 \\ e^{i\beta} \sin \alpha & 0 & e^{-i\beta} \sin \alpha \\ 0 & e^{i\beta} \sin \alpha & -\sqrt{2} \cos \alpha \end{pmatrix},\end{aligned}\quad (14)$$

where

$$V(\mathbf{r}) = \frac{\mu_B B_{\text{tot}}}{\hbar\omega_T} = \frac{\mu_B B_z}{\hbar\omega_T} \sqrt{1 + \frac{G^2 \ell_T^2}{B_z^2} (x^2 + y^2)}. \quad (15)$$

We are now using the notation x and y for the scaled position around the minimum, not to be confused with the original notation. In these rescaled units, one has $\mathbf{p} = -i\nabla$.

With the above definition, it follows that

$$\begin{aligned}\frac{\mu_B B_z}{\hbar\omega_T} &= \frac{\omega_L}{\omega_T} \equiv \rho^{-2}, \\ \frac{G^2 \ell_T^2}{B_z^2} &= \frac{\omega_T}{\omega_L} \equiv \rho^2,\end{aligned}\quad (16)$$

in terms of which

$$V(\mathbf{r}) = \frac{1}{\rho^2} \sqrt{1 + \rho^2(x^2 + y^2)}. \quad (17)$$

The ratio ρ precisely compares the motional dynamics (frequency trap) to the spin dynamics (Larmor frequency). As one can see, the full dynamics of the problem depend only on this single dimensionless parameter. In the usual trapping situation, this is a small parameter, typically ranging from 10^{-3} to 10^{-1} , telling that, (i) the Born-Oppenheimer approximation is valid, and (ii) the trap is almost harmonic $V(\mathbf{r}) \approx \frac{1}{\rho^2} + \frac{1}{2}(x^2 + y^2)$. On the other hand, for $\rho \approx 1$, i.e., the timescale of the spin and the motional dynamics are comparable, deviations from the harmonic behavior are marked and all the effects beyond the Born-Oppenheimer approximation become important, in particular the Majorana's losses.

Finally, as functions of the magnetic field gradient G (in T/m) and the bias field B_z (in μT), one has for Rb⁸⁷:

$$\begin{aligned} \omega_T &= \sqrt{\frac{\mu_B}{M}} \frac{G}{\sqrt{B_z}} = 8.135 \times 10^2 \frac{G}{\sqrt{B_z}} \\ \nu_T &= \frac{\omega_T}{2\pi} = 129.47 \frac{G}{\sqrt{B_z}} \\ \frac{\omega_T}{\omega_L} &= \frac{\hbar}{\sqrt{\mu_B M}} \frac{G}{B_z^{3/2}} = 9.25 \times 10^{-5} \frac{G}{B_z^{3/2}}. \end{aligned} \quad (18)$$

For a given value of G and B_z , the dimensionfull values for frequencies and the decay rates are related to the numerical ones as follows:

$$\begin{aligned} \nu_{\text{exp}} &= \nu_T \times E_{\text{num}}, \\ \frac{\Gamma_{\text{exp}}}{2\pi} &= \nu_T \times \Gamma_{\text{num}}, \end{aligned} \quad (19)$$

see below for application.

III. BEYOND THE BORN-OPPENHEIMER APPROXIMATION

A. Effective Hamiltonian

As mentioned above, beside the vector potentials \mathbf{A}_j and the Born-Huang scalar potentials Φ_j , off-diagonal couplings between the components ψ_j arise because of the motion of the atoms. From a mathematical point of view, this is nothing but saying that the operator $\frac{\mathbf{p}^2}{2}$ does not commute with the position dependent diagonalization of the spin Hamiltonian. More precisely, decomposing the state of the system $|\Psi(\mathbf{r})\rangle$ in the eigenstates of the spin Hamiltonian, $|\Psi(\mathbf{r})\rangle = \sum_j \psi_j(\mathbf{r})|\chi_j(\mathbf{r})\rangle$, one can derive the effective Hamiltonian H_{eff} acting on the

wave functions $\psi_j(\mathbf{r})$. One has

$$\begin{aligned} |\chi_-(\mathbf{r})\rangle &= \sin^2 \frac{\alpha}{2} |1\rangle - \frac{1}{\sqrt{2}} \sin \alpha e^{i\beta} |0\rangle \\ &\quad + \cos^2 \frac{\alpha}{2} e^{2i\beta} |-1\rangle, \\ |\chi_0(\mathbf{r})\rangle &= -\frac{1}{\sqrt{2}} \sin \alpha |1\rangle + \cos \alpha e^{i\beta} |0\rangle \\ &\quad + \frac{1}{\sqrt{2}} \sin \alpha e^{2i\beta} |-1\rangle, \\ |\chi_+(\mathbf{r})\rangle &= \cos^2 \frac{\alpha}{2} |1\rangle + \frac{1}{\sqrt{2}} \sin \alpha e^{i\beta} |0\rangle \\ &\quad + \sin^2 \frac{\alpha}{2} e^{2i\beta} |-1\rangle, \end{aligned} \quad (20)$$

where the $|m\rangle$ are the Zeeman states. The associated eigenvalues are $-V(\mathbf{r})$, 0 and $+V(\mathbf{r})$, respectively.

Assuming that the magnetic field simply reads $(Gx, -Gy, B_z)$, one obtains

$$\begin{aligned} \tan \beta &= -y/x = -\tan \theta \\ \tan \alpha &= \frac{G}{B_z} \sqrt{\tilde{x}^2 + \tilde{y}^2} = \frac{G\ell_T}{B_z} \sqrt{x^2 + y^2} = \rho \sqrt{x^2 + y^2}. \end{aligned} \quad (21)$$

In the adiabatic limit, i.e., $\rho \rightarrow 0$, $\alpha \rightarrow 0$, the trapping state is $|\chi_+(\mathbf{r})\rangle \approx |S_z = 1\rangle$,

In harmonic units, H_{eff} acting on the vector (ψ_+, ψ_0, ψ_-) reads formally as follows:

$$H_{\text{eff}} = \begin{pmatrix} h_{++} & h_{+0} & h_{+-} \\ h_{0+} & h_{00} & h_{0-} \\ h_{-+} & h_{-0} & h_{--} \end{pmatrix} + \begin{pmatrix} V(\mathbf{r}) & 0 & 0 \\ 0 & 0 & 0 \\ 0 & 0 & -V(\mathbf{r}) \end{pmatrix} \quad (22)$$

The diagonal entries take the form

$$h_{jj} = \frac{1}{2}(\mathbf{p} - \mathbf{A}_j)^2 + \Phi_j, \quad (23)$$

where

$$\begin{aligned} \mathbf{A}_+(\mathbf{r}) &= \left(1 - \frac{1}{\gamma}\right) \frac{\mathbf{e}_\theta}{r}, \\ \mathbf{A}_0(\mathbf{r}) &= \frac{\mathbf{e}_\theta}{r}, \\ \mathbf{A}_-(\mathbf{r}) &= \left(1 + \frac{1}{\gamma}\right) \frac{\mathbf{e}_\theta}{r}, \\ \Phi_-(\mathbf{x}) &= 2\Phi_0(\mathbf{x}) = \Phi_+(\mathbf{x}) = \frac{\rho^2(1 + \gamma^2)}{4\gamma^4} \end{aligned} \quad (24)$$

with $r = \sqrt{x^2 + y^2}$ and $\gamma = \gamma(r) = \sqrt{1 + \rho^2 r^2}$.

The off-diagonal entries of H_{eff} are

$$\begin{aligned}
 h_{+0} &= -\frac{\sqrt{2}\rho}{2r\gamma^2} \left(-r \frac{\partial}{\partial r} - i\gamma \frac{\partial}{\partial \theta} \right) + \frac{\sqrt{2}\rho}{2r\gamma^4} (\gamma^3 - \gamma^2 + 1), \\
 h_{+-} &= \frac{r^2 \rho^4}{4\gamma^4}, \\
 h_{0+} &= -\frac{\sqrt{2}\rho}{2r\gamma^2} \left(r \frac{\partial}{\partial r} - i\gamma \frac{\partial}{\partial \theta} \right) + \frac{\sqrt{2}\rho}{2r\gamma^4} (\gamma^3 - 1), \\
 h_{0-} &= \frac{\sqrt{2}\rho}{2r\gamma^2} \left(r \frac{\partial}{\partial r} + i\gamma \frac{\partial}{\partial \theta} \right) + \frac{\sqrt{2}\rho}{2r\gamma^4} (\gamma^3 + 1), \\
 h_{-+} &= \frac{r^2 \rho^4}{4\gamma^4}, \\
 h_{-0} &= -\frac{\sqrt{2}\rho}{2r\gamma^2} \left(r \frac{\partial}{\partial r} - i\gamma \frac{\partial}{\partial \theta} \right) + \frac{\sqrt{2}\rho}{2r\gamma^4} (\gamma^3 + \gamma^2 - 1).
 \end{aligned} \tag{25}$$

H_{eff} is Hermitian with respect to the scalar product $\langle f(r, \theta) | g(r, \theta) \rangle = \iint r dr d\theta f^*(r, \theta) g(r, \theta)$.

B. Numerical implementation

The Hamiltonian H_{eff} is invariant under spatial rotations, therefore the eigenstates can be written as $e^{im\theta}(\psi_+(r), \psi_0(r), \psi_-(r))$. For each value of m , the resulting Hamiltonian H_m only depends on the radial coordinate r . Since the value of the functions $\psi_j(r)$ at $r = 0$ is not fixed by any boundary condition, one uses a discretization scheme that does not contain the point $r = 0$, namely the grid points are $r_n = (n + 1/2)\Delta r$, for n ranging from 0 to a maximum value N . $1/\Delta r$ fixes the number of grid points per harmonic length, whereas $N\Delta r$ corresponds to the size of the system in harmonic length units. The Hamiltonian H_m is Hermitian for the scalar product $\langle F | G \rangle = \int r dr (f_+^*(r)g_+(r) + f_0^*(r)g_0(r) + f_-^*(r)g_-(r))$, where $F = (f_+(r), f_0(r), f_-(r))$, such that it is the discretization of the equation $rH_m\psi = E r\psi$ that leads to a generalized eigenvalue problem $AX = EBX$, where A and B are $(3N + 3) \times (3N + 3)$ Hermitian matrices, B being positive definite.

Neglecting the off-diagonal coupling, the effective potentials seen by ψ_0 and ψ_- components being 0 and $-V(\mathbf{r})$, the corresponding eigenstates are not bound states but scattering states, whereas they are bound states for the ψ_+ component. The off-diagonal coupling allows this bound states to decay to the scattering channels, which, from a mathematical point of view, becomes resonances, i.e., complex poles of the Green function $G(z) = 1/(z - H)$. The complex rotation method is appropriate to compute directly the properties of these resonances (energy, width). Its properties rely on mathematical properties of the analytic continuation of the Green's function in the complex plane [17, 18]. A review of its application to atomic physics can be found in [12].

The method is implemented in our case by making the radial coordinate complex: $r \rightarrow e^{i\phi}r$ and $\frac{\partial}{\partial r} \rightarrow e^{-i\phi}\frac{\partial}{\partial r}$, where ϕ is a real parameter (the rotation angle). The

matrix representations of the Hamiltonian then become complex symmetric, but are no more Hermitian. The fundamental properties of the complex spectra are :

- The bound states, if any, are still on the real axis.
- The continua are rotated by an angle 2ϕ on the lower-half complex plane, around their branching point.
- Each complex eigenvalue E_j gives the properties of one resonance, i.e., the energy is the real part of E_j , and the width is two times the negative of the imaginary part. The complex eigenvalues are independent of ϕ , provided that they are not covered by the continua.

Note that in the present case, the branching point associated to ψ_0 is located at $E = 0$, whereas the one associated to ψ_- is formally at $E = -\infty$, since $-V(r) \approx -r/\rho$ for large r . The scattering states for a linear potential oscillate faster for large distance, such that they cannot be accurately described within a discretization scheme. On the other hand, the overlap with the bound states at very large distance is negligible, so that the exact behavior barely impacts the position and the width of the resonance. Therefore to avoid numerical artifacts and increase the numerical accuracy, we replace the anti-trapping potential for ψ_- by

$$V_{\text{scatt}}(r) = \frac{1}{\rho^2} \sqrt{1 + \rho^2 \frac{r^2}{1 + h^2 r^2}}, \tag{26}$$

where h is a small parameter, typically $h \approx 10^{-2}$. For $hr \ll 1$, then $V_{\text{scatt}}(r) \approx V(r)$, whereas for $hr \gg 1$, then $V_{\text{scatt}}(9r) \approx 1/h\rho$, such that the scattering states have a well defined wavelength for large r values. We have numerically checked that the results presented here are insensitive to the actual h value.

C. Results

The properties of the resonances (position in energy and width) are displayed, as functions of ω_T/ω_L , in Fig. 1 for the $m = 0$ states and in Fig. 2 for the $m = \pm 1$ states. In both cases, the zero of energy corresponds to the bottom of the trapping state, i.e., corresponding to a global shift of $-\frac{1}{\rho^2}$ of the eigenenergies of H_{eff} , such that in the adiabatic limit $\rho \rightarrow 0$, the energies directly correspond to the harmonic oscillator levels. This is clearly seen on the left part of the top plots. On the contrary, for $\rho \approx 1$ (right part), the energy levels differ from the harmonic one, in particular, the difference in energy $E_{n+1} - E_n$ gets smaller with higher n reflecting the linear behavior of the trapping potential $V(r)$ at large r . The behavior in the adiabatic regime can be obtained from the perturbation expansion of h_{++} with respect to \mathbf{A}_+ and ϕ_+ .

More precisely, for a fixed value of m , h_{++} reads:

$$h_{++} = h_{++}^{(0)} - \frac{m}{r^2} \left(1 - \frac{1}{\gamma}\right) + \frac{1}{4r^2} \left(\frac{3\gamma^4 - 4\gamma^3 - 2\gamma^2 + 1}{\gamma^4} \right) \quad (27)$$

where $h_{++}^{(0)} = \frac{p^2}{2}$ when $\rho \rightarrow 0$. The second term arises from the gauge field \mathbf{A}_+ and results in a energy splitting among the $\pm m$ states, which is clearly observed in Fig. 2. A Taylor expansion of these two terms at small distances $\rho r \ll 1$ leads respectively to:

$$\begin{aligned} -\frac{m}{r^2} \left(1 - \frac{1}{\gamma}\right) &\approx -m \left(\frac{\rho^2}{2} - \frac{3}{8} \rho^4 r^2 \right) \\ \frac{1}{4r^2} \left(\frac{3\gamma^4 - 4\gamma^3 - 2\gamma^2 + 1}{\gamma^4} \right) &\approx \frac{\rho^2}{2} - \frac{5}{8} \rho^4 r^2 \end{aligned} \quad (28)$$

The two terms proportional to ρ^2 correspond to an energy shift whereas the two terms proportional to $\rho^4 r^2$ correspond to modification of the trap frequency. However, the preceding formula cannot be compared directly to the numerical results since at large distances $\rho r \gg 1$, the two last terms in h_{++} leads to an effective centrifugal potential $(-m + \frac{3}{4})r^{-2}$, which is independent of ρ . This shows that, although \mathbf{A}_+ and ϕ_+ are small perturbations to the h_{00} , the resulting energy shift has to be computed using their exact expressions, not just their Taylor expansion around $r = 0$. Furthermore, in the adiabatic regime, the decay rates can be obtained from the Fermi golden rule. Assuming that one can approximate the scattering states as plane waves $\psi_0(r) \approx e^{ikr}$, i.e., neglecting the fact that r is a radial coordinate, the decay rates are proportional to the modulus square of the Fourier transform $|\psi_+^{(n)}(k)|^2$ of the harmonic trap wave functions, taken at the k corresponding to the energy of the bound state, i.e., such that $\frac{k^2}{2} = E_n + \frac{1}{\rho^2}$. At first order the decay is dominated by the Gaussian decay of the wave function $e^{-r^2/2}$, such that one has:

$$\Gamma \approx e^{-k^2} = e^{-2E_n - 2/\rho^2}. \quad (29)$$

Therefore, one predicts a linear behavior of $\ln \Gamma$ as functions of $\rho^{-2} = \omega_L/\omega_T$. This can be seen for both $m = 0$ and $m = \pm 1$ states (Figs. 1 and 2, bottom plots).

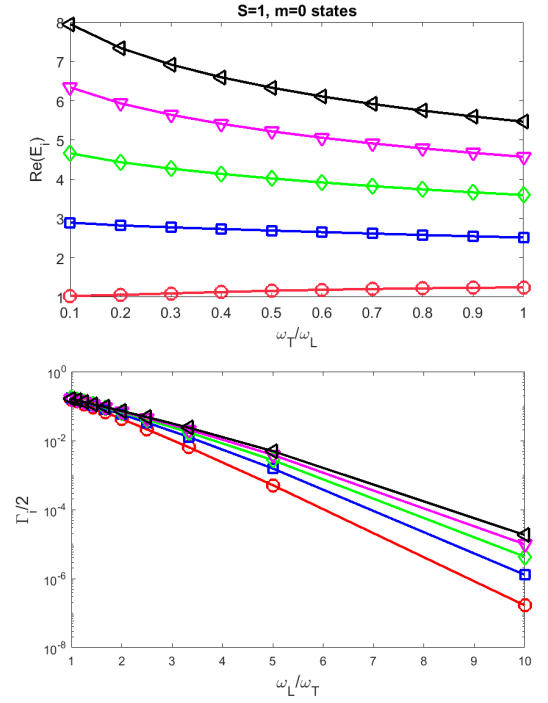


Figure 1. (color online) Properties of the $m = 0$ resonances of the Hamiltonian H_{eff} : positions in energy as functions of ω_T/ω_L (top plot) and decay rates as functions of ω_L/ω_T (bottom plot). A given symbol and color correspond to the same state for the two plots.

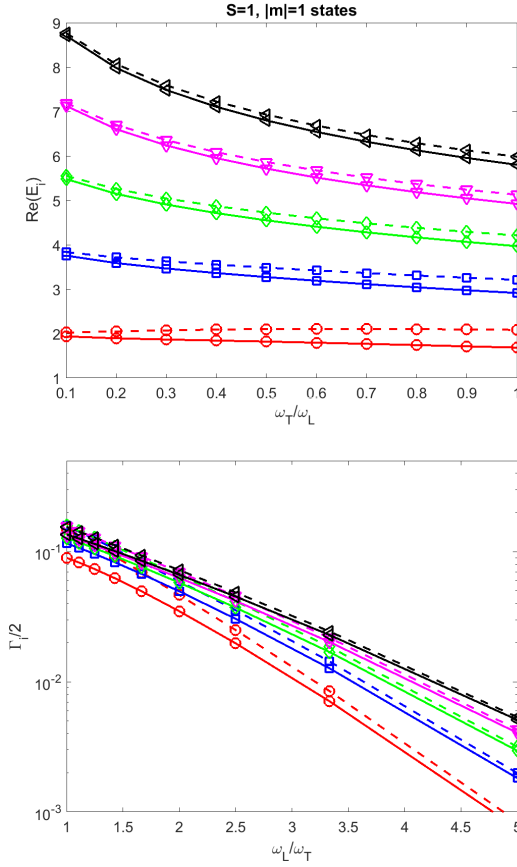


Figure 2. (color online) Properties of the $m = \pm 1$ resonances of the Hamiltonian H_{eff} : positions in energy as functions of ω_T/ω_L (top plot) and decay rates as functions of ω_L/ω_T (bottom plot). The dashed line is for $m = -1$ and the solid line is for $m = 1$. A given symbol and color correspond to the same state for the two plots.

The behavior, at fixed ρ , is slightly more complicated since one has to take into account the exact shape of the harmonic functions, in particular to explain that for small ρ , the decay rates increase with the principal quantum number. We have checked on a simpler model that it is indeed a generic behavior: for a fixed value of ρ , the decay rates depict a maximum around an energy (which depends on ρ), see Fig. 3.

From the numerical point of view, Table I summarizes the expected decay rate of the $m = 0$ ground state and the energy splitting between the first two $m = \pm 1$ states for few values of ω_T/ω_L . From the experimental point of view, for Rb⁸⁷ Fig. 4 displays the life-time $2\pi/\Gamma$ (solid black line) and the gradient G (red dashed line) as functions of the bias field along the z axis, for the four different values of ω_T/ω_L depicted in Table I. For instance, for a value of $\omega_T/\omega_L = 0.2$ (top-left plot), for a bias field value of $5\mu T$, the life-time is $\approx 70\text{ms}$, whereas G is $\approx 25T/m$. For these values, the trap frequency is $\approx 14.5\text{kHz}$. The energy splitting between the ± 1 states is 2.2kHz . The splitting of the energy levels can be measured using RF-spectroscopy on the magnetic trap for a

cold thermal cloud [19].

ω_T/ω_L	0.2	0.25	0.31	0.4
$\Gamma_{\text{num}} \times 10^3$	1.0	4.8	16.0	41.8
$E_{\text{num}}^- - E_{\text{num}}^+$	0.15	0.18	0.21	0.25

Table I. Decay rate of the $m = 0$ ground state and the energy splitting between the first two $m = \pm 1$ states for four values of ω_T/ω_L .

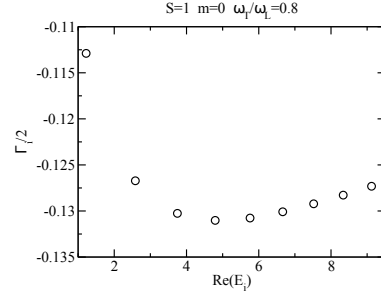


Figure 3. Resonances in the complex energy plane for a fixed value of $\rho^2 = \frac{\omega_T}{\omega_L} = 0.9$. As one can see, around an energy value that depends on ρ , ($E \approx 5$ for $\rho^2 = 0.9$), the imaginary part of the resonances attains a (negative) minimum value, corresponding therefore to a maximum value of the decay rate.

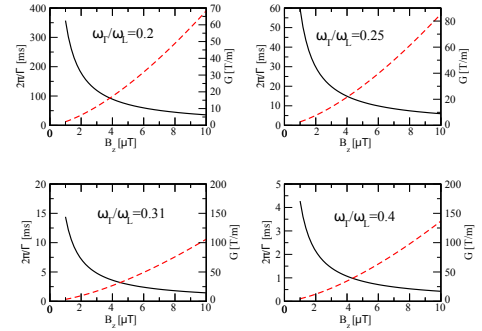


Figure 4. (color online) Lifetime $2\pi/\Gamma$ (solid black line, left axis) and the gradient G (red dashed line, right axis) as functions of the bias field along the z axis, for the four different values of ω_T/ω_L depicted in the Table I. For instance, for a value of $\omega_T/\omega_L = 0.2$ (top-left plot), for a bias field value of $5\mu T$, the life-time is $\approx 70\text{ms}$, whereas G is $\approx 25T/m$. For this value, the trap frequency is $\approx 14.5\text{kHz}$. The energy splitting between the ± 1 states is 2.2kHz .

IV. CONCLUSIONS

We have shown that a tight magnetic trap allows for investigating the break-down of the Born-Oppenheimer

condition. For instance, the adiabatic corrections reduce trap frequencies and the Born-Huang potential counteracts the adiabatic potential. The coupling between trapping and anti-trapping states results in losses which, nevertheless remain experimentally tolerable. In addition, we have shown how molecular Aharonov-Bohm gauge potentials responsible for topological Berry phase effects are emerging. These effects are two-dimensional analogues of the Weyl cones that have been simulated in cold atoms [20]. Within experimentally accessible parameter ranges, i.e. reasonable B_z , one could measure Majorana losses and the splitting between $m = \pm 1$, due to Berry connection and Born-Huang terms characterizing thereby their impact. As a future work, one could study the dynamics of a wave packet, for instance shifting the trap center. Finally, it would be interesting to study the impact of

atom-atom interactions.

ACKNOWLEDGMENTS

The Centre for Quantum Technologies is a Research Centre of Excellence funded by the Ministry of Education and National Research Foundation of Singapore. E. S. acknowledges financial support from the Swedish Research Council (VR) through Grant No. D0413201. The project leading to this publication has received funding from Excellence Initiative of Aix-Marseille University - A*MIDEX, a French “Investissements d’Avenir” program through the IPhU (AMX-19-IET-008) and AMUtech (AMX-19-IET-01X) institutes.

-
- [1] D. Pritchard, Phys. Rev. Lett. **51**, 1336 (1983).
 - [2] J. Fortagh, C. Zimmermann, Rev. Mod. Phys. **79**, 235 (2007).
 - [3] I. Lesanovsky, T. Schumm, S. Hofferberth, L.M. Andersson, P. Krüger, and J. Schmiedmayer, Phys. Rev. A **73**, 033619 (2006).
 - [4] J. R. Anglin, J. Schmiedmayer, Phys. Rev. A **69**, 022111 (2004).
 - [5] R. Franzosi, B. Zambon, E. Arimondo, Phys. Rev. A **70**, 053603 (2004).
 - [6] E. A. Hinds, C. Eberlein, Phys. Rev. A **61**, 033614 (2000).
 - [7] J. Schmiedmayer, A. Scrinzi, Quantum Semiclass. Opt. **8**, 693 (1996).
 - [8] M. V. Berry, R. Lim, J. Phys. A: Math. Gen. **23**, 655 (1990).
 - [9] C. A. Mead, Rev. Mod. Phys. **64**, 51 (1992).
 - [10] J. Dalibard, F. Gerbier, G. Juzeliunas, P. Öhberg, I. B. Spielman Rev. Mod. Phys. **83**, 1523 (2011).
 - [11] N. Goldman, G. Juzeliunas, P. Öhberg, Rep. Prog. Phys. **77**, 126401 (2014).
 - [12] A. Buchleitner, B. Grémaud, D. Delande, J. Phys. B: At. Mol. Opt. Phys. **27**, 2663 (1994).
 - [13] J. Ruseckas, G. Juzeliunas, P. Öhberg, M. Fleischauer, Phys. Rev. Lett. **95**, 010404 (2005).
 - [14] Y. -J. Lin, K. Jiménez-García, I. B. Spielman, Nature (London), **471**, 83 (2011).
 - [15] C. V. Sukumar, D. M. Brink, Phys. Rev. A **56**, 2451 (1997).
 - [16] D. M. Brink, C. V. Sukumar, Phys. Rev. A **74**, 035401 (2006).
 - [17] E. Balslev, J. M. Combes, Commun. Math. Phys. **22**, 280 (1971).
 - [18] Y. K. Ho, Phys. Rep. **99**, 1 (1983).
 - [19] A. G. Martin, K. Helmerson, V. S. Bagnato, G. P. Lafyatis, D. E. Pritchard, Phys. Rev. Lett. **61**, 2431 (1988).
 - [20] D. Suchet et al, EPL, **114**, 26005 (2016).